RSC Advances

ROYAL SOCIETY OF CHEMISTRY

www.rsc.org/advances

Critical formation conditions for β-form hybrid shish-kebab and its structural analysis

Rui Han, Yijun Li, Qi Wang, Min Nie *

Address: State Key Laboratory of Polymer Materials Engineering, Polymer Research Institute of Sichuan University, Chengdu 610065, China

Email: poly.nie@gmail.com

Fax: +86-28-85402465

Tel: +86-28-85405133

* Corresponding author. E-mail: poly.nie@gmail.com

Abstract

In this paper, the critical formation conditions for β-form hybrid shish kebab structure were successfully established based on the temperature/composition diagram of polypropylene (PP)/β nucleating agent (TMB-5). Furthermore, this special structure was subsequently realized in practical PP pipe processing and the multi-level and multi-scale structures were investigated comprehensively by employing various characterization approaches. The results showed that the β-form hybrid shish-kebab structure had a cylindrical symmetry where β-form lamellas were arranged in two different ways along the fibrous nucleating agent: the edge-on lamellae being parallel and the flat-on lamellae being perpendicular to the nucleating agent, indicating the double-orientation of the molecular chains. Moreover, based on the thicker flat-on lamellae and the higher ratio of flat-on to edge-on lamellae in the inner layer with slower cooling, a two order growth mechanism of the β-form hybrid shish-kebab was proposed: flat-on lamellae forming first at high temperature, followed by the formation of edge-on lamellae during the cooling process.

Key words: Controlled crystallization; self-assembly; polypropylene; hybrid shish kebab; crystalline structure

Introduction

The crystalline structure of polymers determines the final performance of a product as much as their chemical structure does [1-6]. Since polymer crystallization is a kinetically controlled process, variations in stress and temperature and the presence of additives all have a significant influence on the final crystalline structure [1, 7, 8]. Therefore, much attention has been directed toward microstructure optimization and property enhancement via controlled crystallization.

A typical representative crystalline polymer, isotactic polypropylene (PP) has two main lamella-stack patterns named spherulite [9] and shish-kebab [10]. As reported, anisotropic shish-kebab can produce property enhancements along the orientation direction in contrast with the isotropic effects of spherulitic morphology. It is well-established that polymer chains orient and stretch in the flow field [11, 12]. Subsequently, the oriented molecules coalesce to form fibrous bundles (shish), which act as a template to promote the epitaxial crystallization of folded-chain lamellae perpendicular to the shish, so as to form the shish kebab structure [13, 14]. However, due to their thermodynamic instability, stretched macromolecules easily relax back to random coils, and only survive in intense stress and quick cooling processing conditions [14, 15].

The final morphology formed in polymer products heavily depends on the topology structure of the nuclei in the early stages of crystallization [16-18]. When fiber-like nuclei with high aspect ratios are introduced into the polymer matrix, the polymer can crystallize epitaxially on the surface and form hybrid shish kebab with an

anisotropic morphology, where the shish is made of fibrous nuclei and the kebabs by polymer [19, 20]. Enlightened by this crucial finding, it is proposed to introduce the fiber-like nuclei into the polymer matrix during its crystallization to tailor nuclei morphology and thus direct the crystallization of the polymer, forming high levels of preferred orientation in the polymer products. Some fibrous nucleating agents were reported to act as templates promoting molecular crystallization on the surfaces via lattice matching, in this way they provide massive possibilities for obtaining the anisotropic morphology named hybrid shish-kebab. For example, dibenzylidene sorbitol (DBS) and its derivatives, the efficient nucleating agents for PP, can dissolve in the polymer melts and upon cooling self-assemble into fibrous structure in a linear fashion [21], further leading PP lamellae to grow oriented epitaxilly on its surface. In the flow field, DBS fibrils lie parallel to the flow direction so their alignment triggers the orientation of PP [22]. This anisotropic morphology led to an enhanced tensile modulus and other useful mechanical properties proved by Lipp [23] and Shepard [24].

Considering the excellent toughness and impact resistance of β-form PP [6], the hybrid shish-kebab crystals rich in β-form are very important for simultaneous reinforcement and toughening of PP products. Recently, several kinds of β-nucleating agents were also found to have a fiber-like morphology in the polymer melt. Varga studied the self-assembly of β nucleating agents (NJS) driven by hydrogen bonds and obtained PP samples with spherulite, fibrous and dendric morphology depending on the initial concentrations and the final heating temperature [25]. Masayuki extruded PP sheets containing NJS and controlled the processing temperature to form the needle

crystals with the β-form parallel to the flow direction and prepared PP sheets with anomalous mechanical anisotropy [26]. The aryl amide-based compound (TMB-5) is another β nucleating agent, which can dissolve in the polymer melt at high temperature and form a fibrous structure before the initial cooling crystallization of PP [27]. By utilizing the self-assembly behaviors, Nie generated hybrid shish kebab crystals rich in the β form and significantly improved the strength and toughness [20]. A comprehensive understanding of the optimal formation of fibrous β nucleating agents and the structural components of the resulting anisotropic crystalline morphology is necessary to explore the functional mechanisms of β-form hybrid shish kebab formation to improve the performance of PP products. However, to the best of the authors' knowledge, a systematic and clear study of these aspects has not been performed.

In this study, TMB-5, a well-developed aryl amide-based β nucleating agent, was chosen as a model and a systematic and clear investigation of its solution and self-assembly behavior in PP melts was carried out in order to construct a phase diagram with a range of concentrations, providing a guide for the adjustment of the processing parameters to obtain the β-form hybrid shish kebab structure in practical PP products. This special morphology was included in PP pipes as a test sample. The multi-level and multi-scale structure of the β-form hybrid shish-kebab was further investigated by using a variety of characterization methods and a corresponding structural model was proposed.

Experimental section

Materials

The polymer used in this study was isotactic polypropylene (Trade name: T30S) by DuShanZi Petrochemical Co., Ltd. Its molecule weight was 3.9×10^5 g/mol and the melting temperature was 164^{o}C.

A β nucleating agent named TMB-5 was purchased from Shanxi Provincial Institute of Chemical Industry, China. As far as we know, it was an aromatic amide derivative with similar chemical structure to N, N' -dicyclohexyl-2,6-naphthalene dicarboxamide [28] (Figure 1).

Sample preparation

PP/TMB-5 composites contained 0.05, 0.1, 0.2, 0.3, 0.5, 1, 2wt% TMB-5 were blended in an internal mixer at a temperature of 180^{o}C and then were used to investigate the melting temperature of the PP crystals and the dissolving temperature of TMB-5.

For the structural analysis of the β-form hybrid shish kebab, a PP pipe containing 0.1wt% concentration of TMB-5 was prepared by using the self-designed polymer pipe extrusion system. The extrusion temperature and the die temperature were set at 235^{o}C and 180^{o}C to generate TMB-5 fibrils. The prepared pipe was named PTC. Its diameter and wall thickness were 32mm and 2mm respectively. As a contrast, a pure PP pipe was extruded as well under the same processing conditions: PC.

Characterization

Polarized light microscopy (PLM).

The melting and phase-transformation behaviors of the blends with the different TMB-5 concentrations, as well as the self-assembly behavior of TMB-5 upon cooling, were carefully observed using a Leica DM2500P polarized light microscope (PLM) equipped with a hot stage(THMS600) at a magnification of 500.

For the prepared pipes, a 10 μm thick slice was cut out along the axial direction from the surface of the pipes to analysis both the morphology and alignment of PP crystals via Leica DM2500P polarized light microscopy (PLM) using a 500x magnification. The observed slice was further heated to 180^{o}C using a Linkam THMS600 heater so that the topological structure of TMB-5 could be clearly seen.

Synchrotron radiation two-dimensional wide-angle X-ray diffraction (2D-WAXD)

The crystal structure of the pipes was characterized by synchrotron 2D-WAXD experiments at the Shanghai Synchrotron Radiation Facility (Shanghai, China). The wavelength was 0.124 nm. The diffraction patterns were recorded with a Mar165 X-ray detector system in transmission mode at room temperature. 2D-WAXD measurement of the specimen was performed in three directions, i.e., extrusion direction (ED), normal to extrusion direction (ND) and transverse-extrusion direction (TD), as illustrated in figure 2.

The relative amount of β crystal was calculated according to the Turner-Jones equation [29]

$$K_{ß} = \frac{I_{ß1}}{I_{ß}+I_{\alpha1}+I_{\alpha2}+I_{\alpha3}} \quad (1)$$

where $I_{ß}$ is the peak intensity of the ß (300) plane, and $I_{\alpha1}$, $I_{\alpha2}$, and $I_{\alpha3}$ are the peak intensity of α (110),α (040),α (130) respectively.

Synchrotron radiation two-dimensional Small-angle X-ray scattering measurement (2D-SAXS)

The arrangement of the lamellae in the prepared pipes was investigated using the synchrotron 2D-SAXS equipment at room temperature in the Shanghai Synchrotron Radiation Facility (Shanghai, China). The sample-to-detector distance was 5m. The background noise was subtracted before quantitative analysis.

Scanning electron microscopy (SEM) observation

The surfaces of the PTC pipes were etched in a 3% mixed acid solution of potassium permanganate at room temperature for 48 h [30], and then washed by diluted sulfuric hydrogen peroxide, and acetone. Finally, the etched surfaces were gold-sputtered for observation using an FEI Inspect F SEM instrument.

Results and discussion

Temperature/composition diagram of PP/TMB-5 blends

The melting temperature of PP and the dissolution temperature of TMB-5 were determined by light microscopy. Typical optical micrographs for PP/TMB-5 blends at different temperatures are presented in figure 3. With increasing temperature, the PP

crystal first melted, then the TMB-5 dissolved into the polymer melt and finally the homogenous solution formed. The melting and dissolution temperatures were recorded when the crystals of PP and TMB-5 disappeared completely. Figure 4 summarizes the phase-transformation temperatures of both PP and TMB-5 as a function of the additive concentration in the range from 0.05wt % to 2wt%. It was observed that the melting temperature of PP remained around 175^{o}C, independent of the composition of the blends. The final melting temperature of PP was determined by the α-form crystals formed due to β to α transition during the heating. In contrast, a pronounced concentration dependence of the dissolution temperature of TMB-5 was found, that is, the dissolution temperature of TMB-5 varied from 210^{o}C to 290^{o}C during the investigated concentrations. When the concentration was lower than 0.2wt%, the dissolution temperature did rise significantly from 210 ℃ to around 270 ℃ while it remained constant at higher concentrations. It can be understood that there is limited liquid miscibility and high solid immiscibility due to the partial polar nature of TMB-5 [31]. Therefore, the solubility of TMB-5 in the polymer melts is dependent on the temperature. Similar results were also investigated for PP/dibenzylidene sorbitol blends [21].

From the composition/temperature diagram for PP/TMB-5 blends, three different physical states were identified. This part mainly focused on the regions above the melting temperature of PP, which involved the formation and evolution of nuclei in the sequent crystallization of PP. This was key to obtain highly-ordered crystalline structure to optimize the microstructure for high-performance PP products. Three

representative temperatures were chosen to reveal the topology of the nucleating agent, which was visualized during the cooling process of the blends with different concentrations of TMB-5 using optical light microscopy. TMB-5 morphologies controlled by the final melting temperature and composition and are shown in figure 5. When the temperature was lower than the dissolving temperature of TMB-5, TMB-5 retained its original point-like shape. At the dissolving temperature, with the cooling homogeneous liquid, prior to PP crystallization the TMB-5 molecules self-assembled into fibrils driven by their hydrogen bonds. At temperatures exceeding the dissolving temperature, fibrous TMB-5 branched and a three-dimensional dendritic structure evolved from the melt due to the perfect crystallization conditions. Moreover, it is interesting to note that the self-assembling topology of TMB-5 was not closely related to the concentration, i.e., in the given temperature regions, they were almost the same except for the increasing density of the resulting structure. This further confirmed that the key factor affecting the nuclei morphology was the solubility of TMB-5. Obviously, fibrous TMB-5 could be obtained only when it recrystallized from the PP melt upon cooling from its phase transformation temperature.

Since TMB-5 is an efficient β nucleating agent for PP, polymer chains tend to nucleate and grow at its surface, that is, the final β-form crystal morphology can be determined by the topology structure of TMB-5. Apparently, β-form hybrid shish kebab crystalline structure can be generated by controlling the final melting temperature and the concentration of TMB-5, as is shown in figure 6.

Formation of β-form hybrid shish kebab in practical processing and its structural analysis

Based on the composition/temperature diagram for PP/TMB-5 blends, PP pipes with 0.1wt% TMB-5 were extruded at 235^{o}C with TMB-5 appearing with a fibrous morphology, inducing the formation of β-form hybrid shish kebab crystalline structure. This process was verified as successful via the picture of figure 7a. In the prepared pipe with the presence of TMB-5, the denser needle-like β crystals could be easily identified and they all aligned along the extrusion direction of the pipe. When the temperature was heated to 180^{o}C, PP crystals melted while TMB-5 kept its solid state. Nucleating agents with fibrous structures are displayed in figure 7b. It is well understood that like conventional shish kebab, the fibrous β nucleating agent acted as a template to replace the oriented molecules (shish) to induce the epitaxial crystallization of PP on the surface, forming β-form hybrid shish-kebab. Since the shish composed of extended molecules was unstable and easily relaxed back to a random coil state, especially at high temperature [32], pure PP tended to form isotropic spherulites, as shown in figure 7c. Therefore, the formation of hybrid shish-kebab was thought to be a novel method for preparing high-performance PP products in a practical process [20]. Obviously, comprehensive understanding of this anisotropic structure was essential. In this section, the micro-structure on different scales were described and analyzed using several approaches.

Firstly, 2D-WAXD was utilized to investigate the β-form hybrid shish-kebab on the scale of the crystalline cell. As illustrated in figure 2, the specimen was measured

in three geometrical states. Clearly, each of 2D-WAXD patterns consisted of five diffraction rings associated with different lattice planes of PP: (110), (300), (040), (130) and (111) [29] from inner to outer circles, respectively. Based on circularly integrated intensities of the planes, 1D-WAXD curves were obtained. As shown in figure 9, the diffraction angle of the β (300) plane at $2\theta=12.8°$ had a much greater intensity than the characteristic peaks of α planes. This indicated that the β-form of the crystal dominated. Using the Turner-Jones Equation, the relative amount of β crystal in PTC was calculated to be 80.4%. This should be ascribed to the selective nucleating effect of TMB-5 on the β-form crystals of PP. Because the sample only contained few α-form crystals, the following discussion mainly focuses on the morphology of the β-form crystals.

It should be noted that in the TD-ND plane the circular pattern of (300) planes was clearly seen while six-arcs patterns appeared in ED-TD plane and ED-ND plane. This implied that the β-form hybrid shish-kebab had a cylindrical symmetry structure where β crystals with mixed multi-modal orientation were arranged along the fibrous nucleating agent. Interestingly, (300) reflection consisted of 6 arcs: equatorial direction, ±30 and ±150^{o} off the meridianal direction, which was also investigated by other researchers [9, 33]. Masayuki ascribed the non-uniform (300) diffraction pattern to the lamellae oriented perpendicularly to the fibrous β nucleating agent with a slight distortion [34]. Liu considered the oriented β lamellas had a similar topology with the α-modified “parent-daughter” lamellae [35]. However, based on the growth mechanism of the β crystals that the lamellae were arranged radially, the "cross-hatched" structure

could not be obtained [36]. Therefore, the fine structures at the lamellar level need to be further investigated.

The visualized information corresponding to the lamellar arrangement could be obtained by SEM. Since the organic nucleating agent was hardly resistant to the etchant, it was removed first. The array of the grooves in figure 10a, b and the holes in figure 10c indicate the nucleating agents. Considering the spatial relationship of figure 10a-c, it is suggested that the lamellae stacked on both sides of the fibrous nucleating centers, resulting in the oriented β lamellas having a cylindrical symmetry, which is typical hybrid shish-kebab with the fibrous nucleating agent equivalent to the "shish" [37]. High-magnification SEM presented a more refined microstructure of the lamellar arrangement in the anisotropic morphology. As shown in figure 11, two different kinds of β arranged crystals, namely plate-like and rod-like structures, were investigated. The former was recognized as oriented flat-on lamellae with the molecular chains oriented perpendicularly to the nucleating agent while the latter was oriented edge-on lamellae with molecular chains parallel to the nucleating agent. This indicated that the double-orientation of molecular chains was developed in the hybrid shish-kebab morphology. It is understood that the presence of the 6-arcs of the (300) plane as shown in figure 8: the arcs in the equatorial direction resulted from the edge-on lamellas and the arcs at ±30 and ±150^{o} off the meridianal direction were produced by the flat-on oriented lamellae where a and b-axes rotated around the molecular orientation.

2D-SAXS was also used to investigate this kind of texture structure in the outer

layer of the PP pipe. As shown in figure 12, two pairs of scattering spots located along equatorial and meridianal directions were clearly observed. These are analogous to the "parent-daughter" lamellas found in the α-modified PP [38]. However, based on the SEM results, the "cross-hatched" morphology should be ascribed to a mixture of both flat-on and edge-on oriented lamellas. The two oriented lamellas grew independently without any hypotaxis. Considering the SAXS beam vertical to the sample, the meridianal scattering spots belonged to the edge-on oriented lamellas while the flat-on oriented lamellas caused the equatorial scattering.

In order to quantitatively compare the concentration of the two oriented lamella in the β-form hybrid shish-kebab, the Lorentz-corrected 1D-SAXS intensity as the function of q ($q = \frac{4\pi}{\lambda}\sin\theta$, where 2θ is the scattering angle and λ the wavelength) was presented in figure 13. The intensities along both the equatorial and the meridianal directions were integrated and the results are listed in Table 1. The scattering intensity along the equatorial direction corresponding to the flat-on lamellae was stronger than that along the meridianal direction which resulted from edge-on lamellas, and implied that the flat-on lamella was dominant in the hybrid shish-kebeb crystal. This finding was in accordance with the above SEM results of more flat-on lamellas.

Additionally, the position of the scattering peak shifted to a lower q in the flat-on lamellae compared to that of the edge-on lamellae. The long period (L) is related to the position of the scattering peak and can be calculated using Bragg's law:

$$L = \frac{2\pi}{q_{max}}$$

Obviously, the long period of the edge-on lamellae is significantly shorter than that of flat-on lamellae. By further applying a 1D electron density correlation function (as shown in figure 14), the corresponding amorphous thickness (d_a) and lamellae thickness (d_c) are obtained [39].

$$K(z) = \frac{\int_0^\infty I(q)q^2 \cos(qz)dq}{\int_0^\infty I(q)q^2 dq}$$

where z is the real space length parameter and I(q) is the 1D intensity distribution.

As can be seen from table 2, the flat-on lamellae is thicker than the edge-on lamellae.

Formation mechanism of the β-modification hybrid shish-kebab

It is well accepted that the nucleating agent plays a role in polymer crystallization. It can control the formation of the initial nuclei and the subsequent lamellae development around the nucleating agent. TMB-5 is a highly efficient nucleating agent for the β-form PP, and can dissolve into the polymer melts at high temperature and self-assemble into the fibril. Due to the favorable lattice matching between TMB-5 and PP, polymer chains "prefer" to nucleate and grow into hybrid shish kebab composed of β-form crystals. However, the lamellar growth depends on the temperature. The flat-on lamellae developed predominately at high temperature while the edge-on lamellae was preferred below the critical temperature [40, 41]. Extrusion of PP pipe was nonisothermal crystallization processing [42]. During cooling, the flat-on lamellae forms first, followed by the edge-on lamellae. Therefore, the final hybrid shish kebab crystals contain the two differently orientated lamellas. The two

order growth mechanism could be confirmed by the thicker flat-on lamellae which was formed at high temperature.

The other evidence for the formation mechanism could come from a comparison between the outer layer and inner layer of PP pipe. Figure 15 was the Lorentz-corrected 1D-SAXS intensity profile from 2D-SAXS of the PP pipe's inner layer and the related results are listed in Table 2. The ratio of the scattering intensity of the flat-on and edge-on lamellas was 1.88, much larger than the 1.22 of outer layer. In the extrusion process, the pipe was cooled by the water spray on the outer surface while the inner layer was cooled by the heat loss from the external wall, producing a much faster cooling rate in the outer wall of the pipe than that of the inner wall. Obviously, the polymer in the inner layer had more residence time at the high temperature, resulting in more flat-on lamellas.

Therefore, it was reasonable to pronounce that the formation of the β-form hybrid shish-kebab crystals was markedly affected by the multiple effects produced by the β fibrous nucleating agent and the thermal history. As a result, two kinds of oriented β lamellas were generated, as illustrated in figure 16.

Conclusions

In this paper, the binary phase diagram of the PP/TMB-5 blends was constructed and the critical forming conditions for fibrous TMB-5 were established. The results suggest that TMB-5 could self-assemble into a fibrous topology upon cooling only when the final heating temperature was precisely controlled around the dissolving

temperature in the PP melt, providing a guide to adjust processing parameters to induce the growth of a β-form hybrid shish kebab crystalline structure.

Additionally, the β-form hybrid shish kebab structure was successfully achieved in practical pipe processing under the guidance of PP/TMB-5 binary phase diagram, and its multi-level structure was investigated. The 2D-WAXD and SEM results revealed that the anisotropic structure with the rich β-form crystals oriented along the extrusion direction and the lamellas were distributed in a cylindrically-symmetry. The 2D-SAXS as well as the high-magnification SEM results further suggested that the lamellas as flat-on and edge-on modes were arranged in parallel and perpendicular to the nucleating agent, resulting in molecular orientation along the extrusion and transverse directions. As a result, a two order growth mechanism for the β-form hybrid shish kebab was proposed: the flat-on lamellae firstly formed at high temperature, followed by the edge-on lamellae during the cooling. Based on the sensitivity of the two kinds of lamellas to temperature, molecular orientation and condensed state structure of β-form hybrid shish kebab are expected to be controlled by tuning thermal history in the processing, which opens a novel and powerful way to tailor the property of polymer products.

Acknowledgement

The authors greatly acknowledge the financial support of the National Nature Science Foundation of China (51127003, 51303114 and 51121001) and the Doctoral fund of Ministry of Education of China (20130181120056). Synchrotron 2D-WAXD and

2D-SAXS experiments were supported by Shanghai Synchrotron Radiation Facility.

Reference

1. Z. Ma, L. Balzano, T. van Erp, G. Portale and G. W. M. Peters, *Macromolecules*, 2013, 9249.
2. N. J. Mills, Plastics Microstructure and Applications; Arnold: Burlington, Canada,1986.
3. A. Galeski, *Prog Polym Sci*, 2003, **28**, 1643.
4. F. Deplace, Z. Wang, N. A. Lynd, A. Hotta, J. M. Rose, P. D. Hustad, J. Tian, H. Ohtaki, G. W. Coates, F. Shimizu, K. Hirokane, F. Yamada, Y.-W. Shin, L. Rong, J. Zhu, S. Toki, B. S. Hsiao, G. H. Fredrickson and E. J. Kramer, *J Polym Sci., Part B: Polym Phys*, 2010, **48**, 1428.
5. P. D. Coates, P. Caton-Rose, I. M. Ward and G. Thompson, *Sci China Chem*, 2013, **56**, 1017.
6. J. Varga, *J Macromol Sci, Part B*, 2002, **41**, 1121.
7. A. J. Lovinger, J. Chua and C. C. Gryte, *J Polym Sci, Polym Phys Edi*, 1977, **15**, 641.
8. H. Li and S. Yan, *Macromolecules*, 2011, **44**, 417.
9. D. R. Norton and A. Keller, *Polymer*, 1985, **26**, 704.
10. A. J. Pennings and A. M. Kiel, *Kolloid-Z.u.Z, Polymere*, 1965, **205**, 160.
11. J. Bent, L. R. Hutchings, R. W. Richards, T. Gough, R. Spares, P. D. Coates, I. Grillo, O. G. Harlen, D. J. Read, R. S. Graham, A. E. Likhtman, D. J. Groves,

T. M. Nicholson and T. C. B. McLeish, *Science*, 2003, **301**, 1691.

12. T. T. Perkins, D. E. Smith and S. Chu, *Science*, 1997, **276**, 2016.
13. S. Kimata, T. Sakurai, Y. Nozue, T. Kasahara, N. Yamaguchi, T. Karino, M. Shibayama and J. A. Kornfield, *Science*, 2007, **316**, 1014.
14. T. Yan, B. Zhao, Y. Cong, Y. Fang, S. Cheng, L. Li, G. Pan, Z. Wang, X. Li and F. Bian, *Macromolecules*, 2010, **43**, 602.
15. R. H. Somani, L. Yang, L. Zhu and B. S. Hsiao, *Polymer*, 2005, **46**, 8587.
16. Rajesh H. Somani, Benjamin S. Hsiao and A. Nogales, *Macromolecules*, 2000, **33**, 9385.
17. R. H. Somani, L. Yang, L. Zhu and B. S. Hsiao, *Polymer*, 2005, **46**, 8587.
18. Yoshiko Ogino, Hajime Fukushima, Nobuaki Takahashi, Go Matsuba, Koji Nishida and T. Kanaya*, *Macromolecules*, 2006, **39**, 7617.
19. N. Ning, F. Luo, B. Pan, Q. Zhang, K. Wang and Q. Fu, *Macromolecules*, 2007, **40**, 8533.
20. M. Nie, R. Han and Q. Wang, *Ind Eng Chem Res*, 2014, **53**, 4142.
21. A. Thierry, B. Fillon, C. Straup, B. Lotz and J. C. Wittmann, *Prog Colloid Polym Sci* 1992, **87**, 28.
22. Luigi Balzano, G. Portale, G. W. M. Peters and S. Rastogi, *Macromolecules*, 2008, **41**, 5350.
23. J. Lipp, M. Shuster, G. Feldman and Y. Cohen, *Macromolecules*, 2007, **41**, 136.
24. T. A. Shepard, C. R. Delsorbo, R. M. Louth, Jonathan L. Walborn, D. A.

Norman, N. G. Harvey And R. J. Spontak, *J Polym Sci, Part B: Polym Phys*, 1997, **35**, 2617

25. J. Z. Varga and A. D. Menyha ŕD, *Macromolecules*, 2007, **40**, 2422.

26. P. Phulkerd, S. Nobukawa, Y. Uchiyama and M. Yamaguchi, *Polymer*, 2011, **52**, 4867.

27. M. Dong, Z. Guo, J. Yu and Z. Su, *J Polym Sci, Part B: Polym Phys*, 2008, **46**, 1725.

28. M. Dong, M. Y. Jia, Z. X. Guo and J. Yu, *J Polym Sci, Part B: Polym Phys*, 2011, **29**, 308.

29. A. Turner Jones, J. M. Aizlewood And D. R. Beckett, *Macromol Chem Phys*, 1963, 134.

30. Jemyung Park, Kyuyoung Eom, O. Kwon and S. Woo, *Microsc. Microanal*, 2001, **7**, 276.

31. C. Ziwei, Z. Yao, L. Jingqing, S. Yingrui, H. Hong, F. Jiachun, S. S. Funari and J. Shichun, *J Appl Polym Sci*, 2013, **128**, 628.

32. R. H. Somani, I. Sics and B. S. Hsiao, *J Polym Sci, Part B: Polym Phys*, 2006, **44**, 3553.

33. R. J. Samuels And R. Y. Yee, *J Polym Sci, Part A-2: Polym Phys*, 1972, **10**, 385.

34. M. Yamaguchi, T. Fukui, K. Okamoto, S. Sasaki, Y. Uchiyama and C. Ueoka, *Polymer*, 2009, **50**, 1497.

35. X. Liu, K. Dai, X. Hao, G. Zheng, C. Liu, D. W. Schubert and C. Shen, *Ind.*

Eng Chem Res, 2013, **52**, 11996.

36. J. Varga, *J Mater Sci*, 1992, **27**, 2557.

37. N. Ning, S. Fu, W. Zhang, F. Chen, K. Wang, H. Deng, Q. Zhang and Q. Fu, *Prog Polym Sci*, 2012, **37**, 1425.

38. P. W. Zhu and G. Edward, *J Mater Sci*, 2008, **43**, 6459.

39. G. R. Strobl, M. J. Schneider And I. G. Voigt-Martin, *J Polym Sci, Polym Phys Edi*, 1980, **18**, 1361.

40. J. P. Yang, Q. Liao, J. J. Zhou, X. Jiang, X. H. Wang, Y. Zhang, S. D. Jiang, S. K. Yan and L. Li, *Macromolecules*, 2011, **44**, 3511.

41. Y. X. Liu and E. Q. Chen, *Coordin Chem Rev*, 2010, **254**, 1011.

42. M. Nie, S. Bai and Q. Wang, *J Appl Polym Sci*, 2011, **119**, 1659.

Table 1 Structural Parameters and integrated intensity obtained from 2D-SAXS of outer layer of PTC

	L (nm)	d_a (nm)	d_c (nm)	I (a.u.)
Flat-on lamellae	18.18	6.25	11.93	13.00
Edge-on lamellae	16.64	6.24	10.40	10.66

Table 2 Structural Parameters and integrated intensity obtained from 2D-SAXS of inner layer of PTC

	L (nm)	I (a.u.)
Flat-on lamellae	19.08	11.2
Edge-on lamellae	15.13	6.22

Figure caption

Figure 1 Chemical structure of N, N'-Dicyclohexyl-2,6-naphthalenedicarboxamide.

Figure 2 2D-WAXD and 2D-SAXS geometry for the extruded pipes.

Figure 3 Typical photographs of the PP/TMB-5 blends during the heating process: (A) T=40^{o}C, 0.1%wt TMB-5; (B) T=200^{o}C; (C) T=240^{o}C.

Figure 4 Temperature /composition diagram of the PP/TMB-5 blends. In the diagrams, the symbols refer to the melting temperature of PP (●) and the dissolution temperature of TMB-5 (■). The letter T refers to TMB-5, P to PP, S to solid, L to liquid.

Figure 5 Typical crystalline structures of TMB-5 at the different final temperatures (T_f) and composite constitutions: (A) 0.1wt% TMB-5, T_f=200^{o}C; (B) 0.1wt% TMB-5, T_f=235^{o}C; (C) 0.1wt% TMB-5, T_f=255^{o}C; (D) 0.5wt% TMB-5 T_f=270^{o}C.

Figure 6 β-form hybrid shish kebab crystalline structure induced by fibrous TMB-5.

Figure 7 PLM photos of the PTC before (a) and after (b) heating to 180^{o}C and (c) PLM picture of the as-prepared PC.

Figure 8 2D-WAXD pattern of PTC pipe at (a) ED-TD plane; (b) ED-ND plane; (c) TD-ND plane.

Figure 9 1D WAXD curves extracted from the 2D-WAXD (ED-TD plane) pattern of PTC.

Figure 10 SEM micrographs of PTC at: (a) ED-TD plane; (b) ND-ED plane; (c) ND-TD plane.

Figure 11 High-magnification SEM micrograph of PTC.

Figure 12 2D-SAXS pattern of outer layer of PTC (ED-TD plane).

Figure 13 Lorentz-corrected 1D-SAXS intensity profiles extracted from figure 7.

Figure 14 One-dimensional electron density correlation function for edge-on and flat-on lamellas.

Figure 15 Lorentz-corrected 1D-SAXS intensity profile extracted from the inner-layer 2D-SAXS pattern of PTC.

Figure 16 Schematic diagram of the lamella orientation in β-modification hybrid shish-kebab.

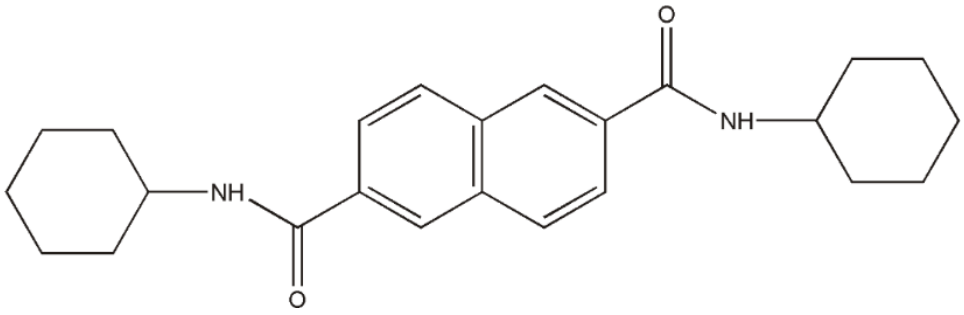

Fig. 1 Chemical structure of N, N'-Dicyclohexyl-2,6-naphthalenedicarboxamide.

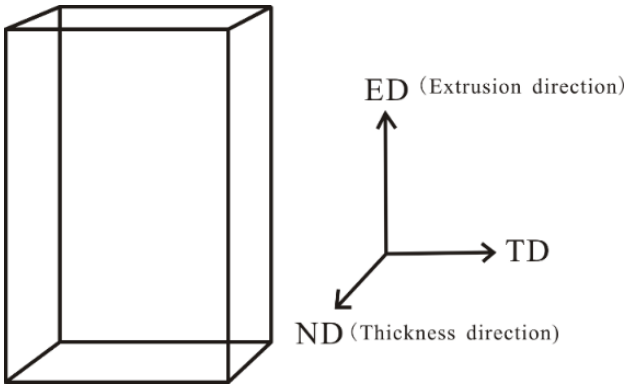

Fig. 2 2D-WAXD and 2D-SAXS geometry for the extruded pipes.

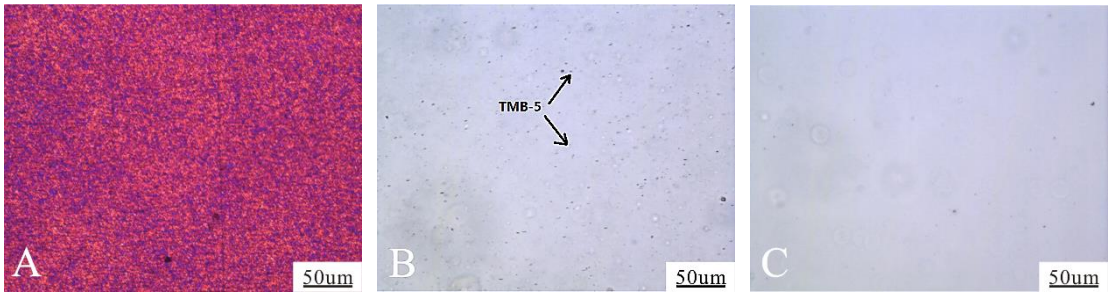

Fig. 3 Typical photographs of the PP/TMB-5 blends during the heating process: (A) T=40°C, 0.1%wt TMB-5; (B) T=200°C; (C) T=240°C.

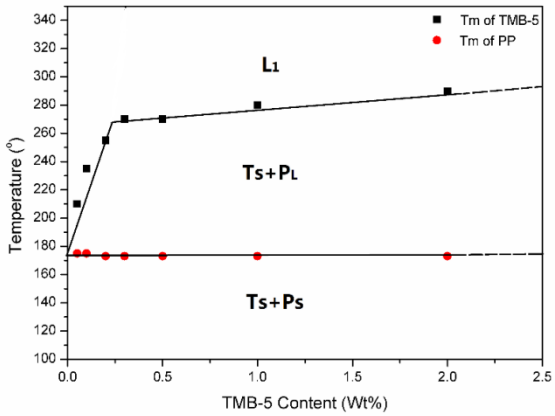

Fig. 4 Temperature /composition diagram of the PP/TMB-5 blends. In the diagrams, the symbols refer to the melting temperature of PP (●) and the dissolution temperature of TMB-5 (■). The letter T refers to TMB-5, P to PP, S to solid, L to liquid.

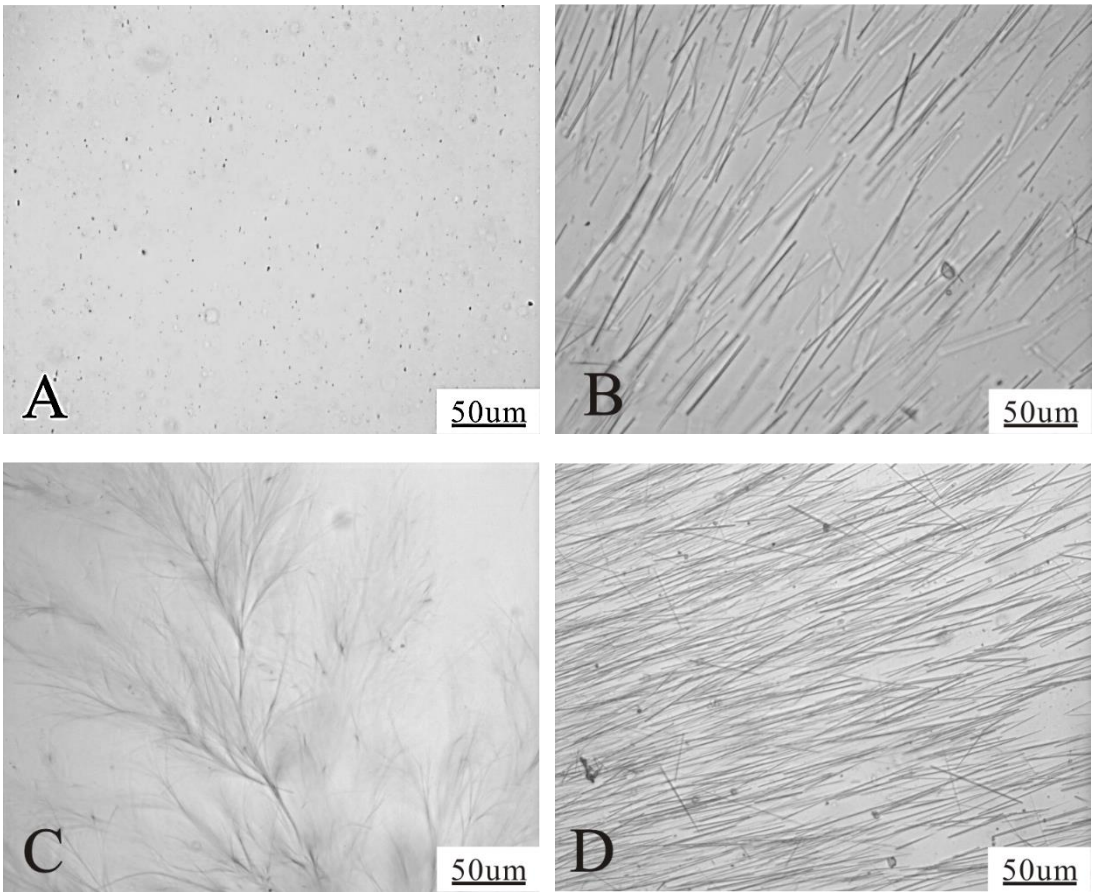

Fig. 5 Typical crystalline structures of TMB-5 at the different final temperatures (T_f) and composite constitutions: (A) 0.1wt% TMB-5, T_f=200^{o}C; (B) 0.1wt% TMB-5, T_f=235^{o}C; (C) 0.1wt% TMB-5, T_f=255^{o}C; (D) 0.5wt% TMB-5 T_f=270^{o}C.

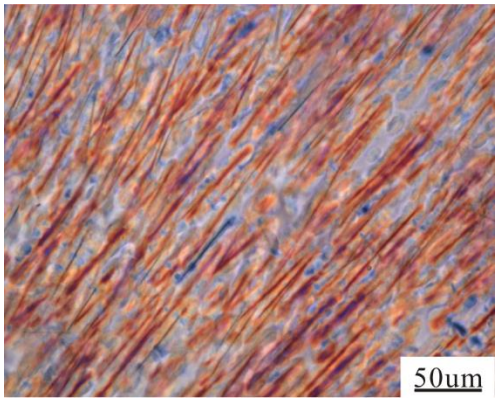

Fig. 6 β-form hybrid shish kebab crystalline structure induced by fibrous TMB-5.

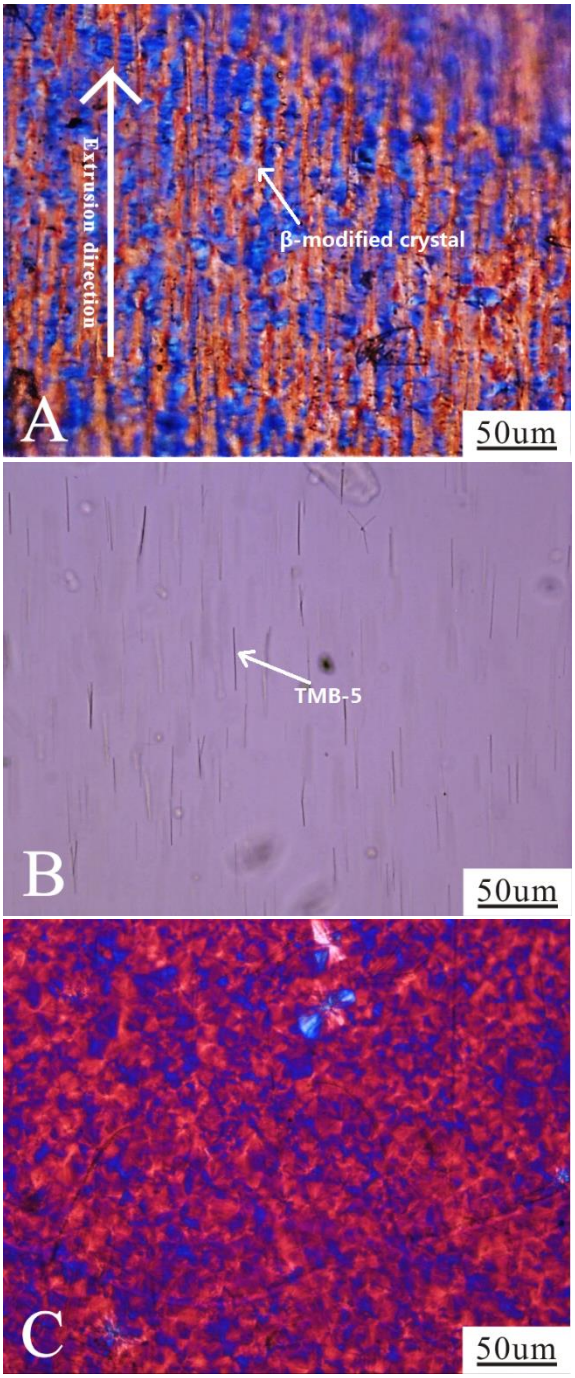

Fig. 7 PLM photos of the PTC before (a) and after (b) heating to 180°C and (c) PLM picture of the as-prepared PC.

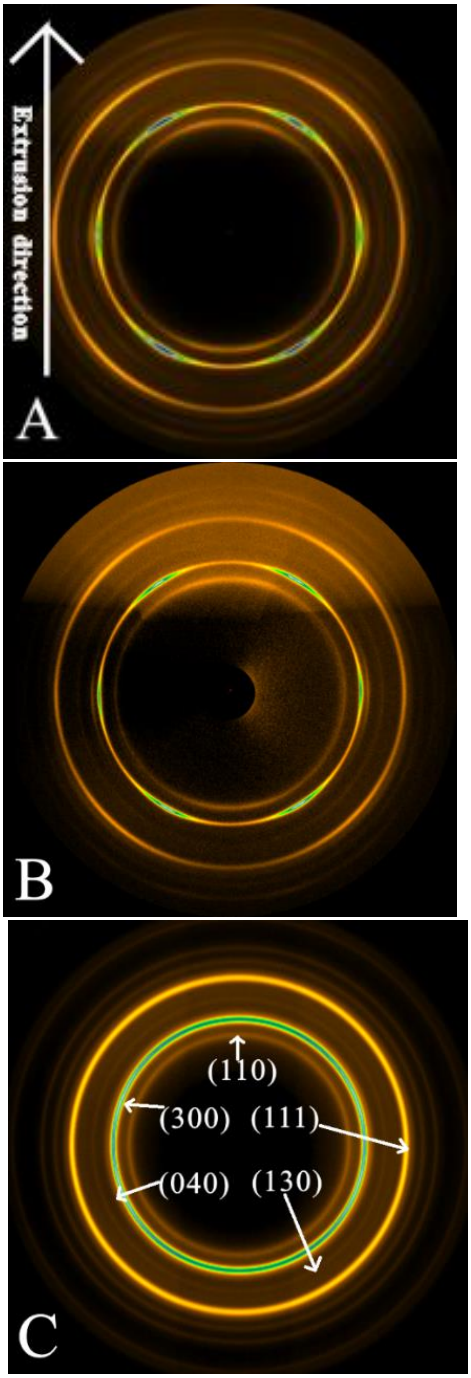

Fig. 8 2D-WAXD pattern of PTC pipe at (a) ED-TD plane; (b) ED-ND plane; (c) TD-ND plane.

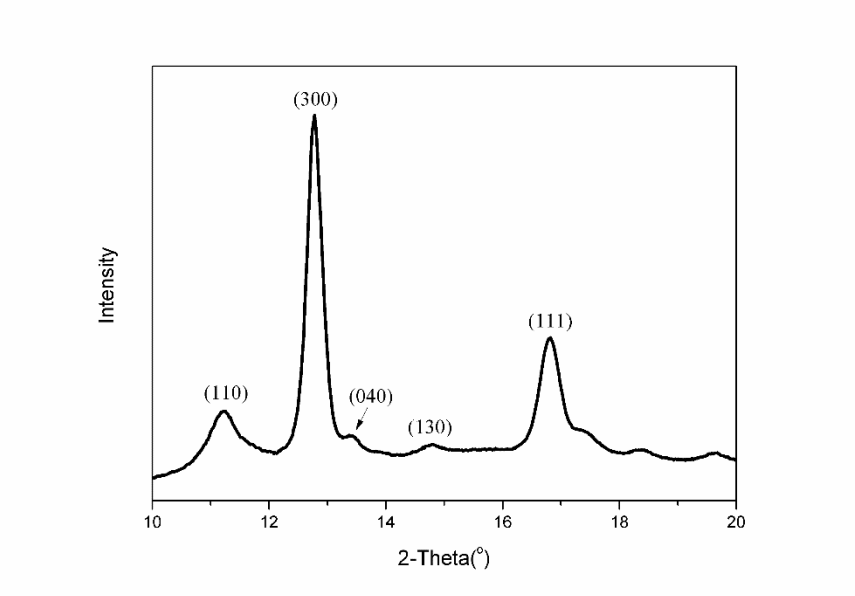

Fig. 9 1D WAXD curves extracted from the 2D-WAXD (ED-TD plane) pattern of PTC.

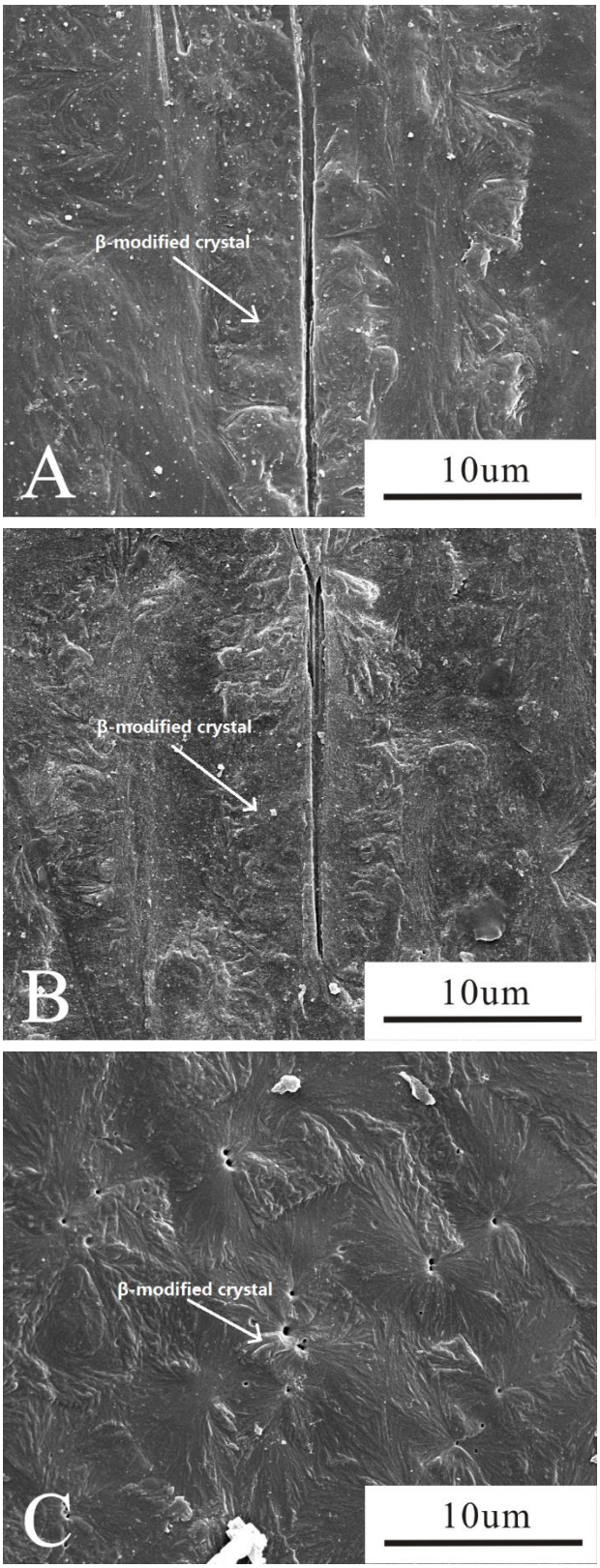

Fig. 10 SEM micrographs of PTC at: (a) ED-TD plane; (b) ND-ED plane; (c) ND-TD plane.

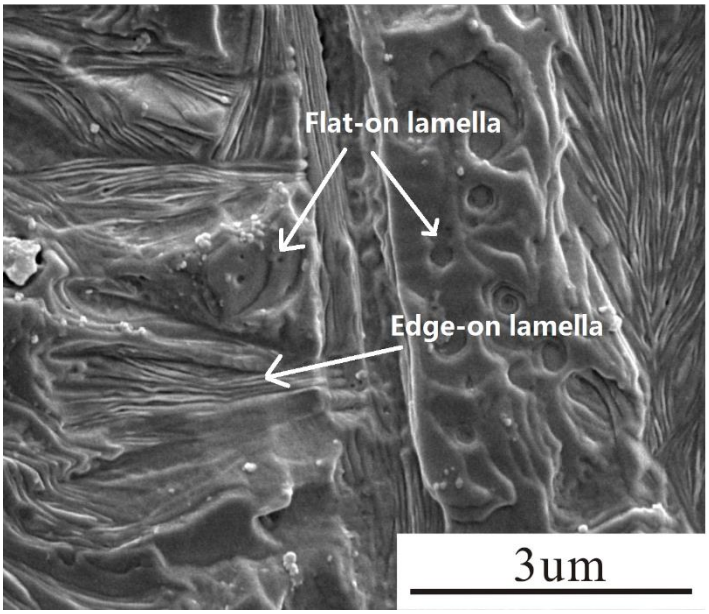

Fig. 11 High-magnification SEM micrograph of PTC.

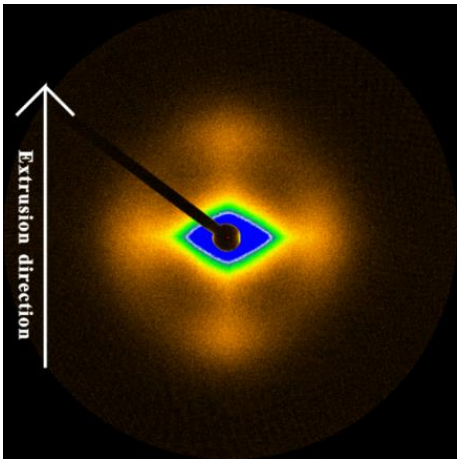

Fig. 12 2D-SAXS pattern of outer layer of PTC (ED-TD plane)

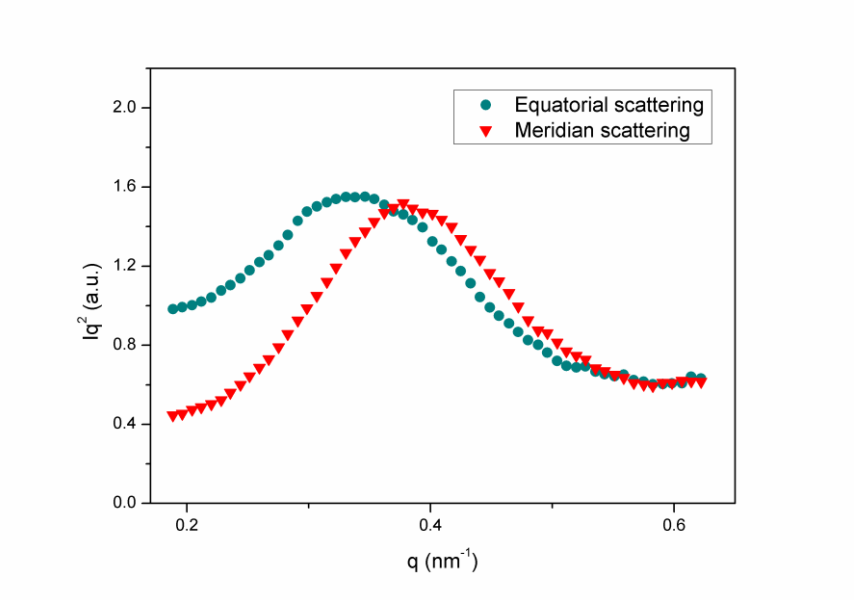

Fig. 13 Lorentz-corrected 1D-SAXS intensity profiles extracted from figure 7.

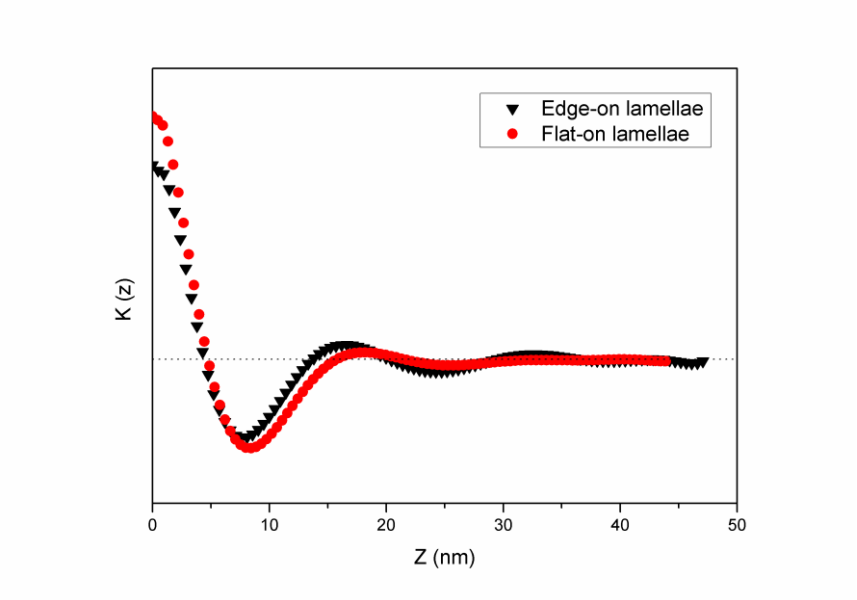

Fig. 14 One-dimensional electron density correlation function for edge-on and flat-on lamellas.

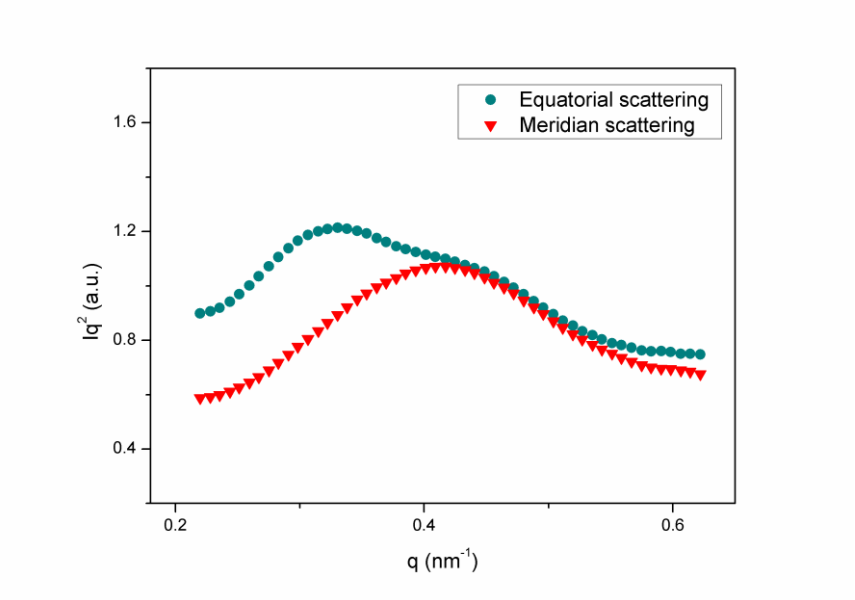

Fig. 15 Lorentz-corrected 1D-SAXS intensity profile extracted from the inner-layer 2D-SAXS pattern of PTC.

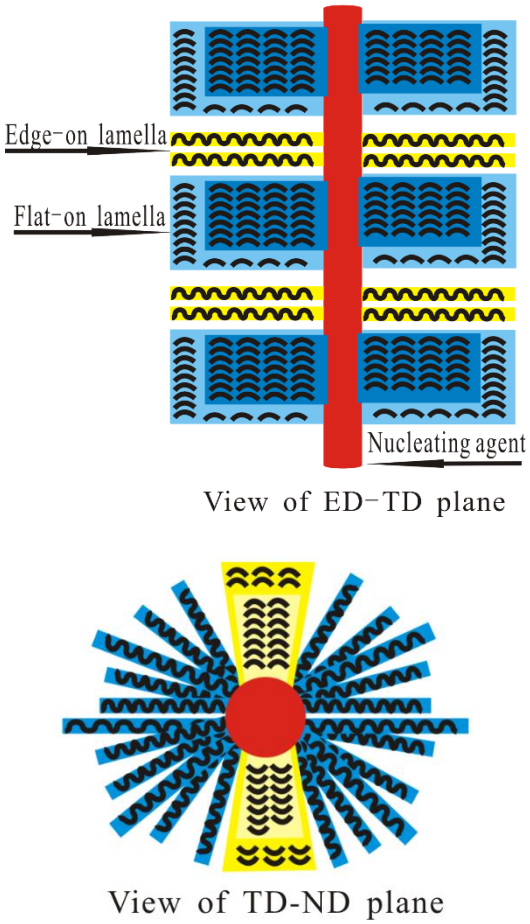

Fig. 16 Schematic diagram of the lamella orientation in β-modification hybrid shish-kebab.